IIT, Bombay

B.Tech. Project
Spring 2016

Density Matrix Renormalization Group using Matrix Product State Ansatz

Author:
Ankit Mahajan
Roll No. 120100027

Supervisor:
Prof. Alok Shukla

Declaration

I, Ankit Mahajan, understand that plagiarism is defined as any one or the combination of the following:

1. Uncredited verbatim copying of individual sentences, paragraphs or illustrations (such as graphs, diagrams, etc.) from any source, published or unpublished, including the internet.

2. Uncredited improper paraphrasing of pages or paragraphs (changing a few words or phrases, or rearranging the original sentence order)

3. Credited verbatim copying of a major portion of a paper (or thesis chapter) without clear delineation of who did or wrote what. (Source: IEEE, The Institute, Dec. 2004)

I have made sure that all the ideas, expressions, graphs, diagrams, etc., that are not a result of my work, are properly credited. Long phrases or sentences that had to be used verbatim from published literature have been clearly identified using quotation marks. I affirm that no portion of my work can be considered as plagiarism and I take full responsibility if such a complaint occurs. I understand fully well that the guide of the seminar report may not be in a position to check for the possibility of such incidences of plagiarism in this body of work.

Abstract

In this project I studied the density matrix renormalization (DMRG) technique as applied to quantum chemical electronic structure calculation. The matrix product state (MPS) ansatz, which entails a matrix product representation of the multi electronic wavefunction and the Hilbert space operators, makes it possible to implement this technique numerically. I did benchmark calculations of ground and low lying excited states of all-trans polyenes (also known as trans polyacetylene or t-PA) up to $C_{18}H_{38}$, using the semi-empirical Pariser-Parr-Pople (PPP) Hamiltonian model. The DMRG results compare favorably with full CI calculations.

In the first chapter the concept of correlation is discussed first followed by a brief historical account of DMRG as introduced by White[14]. The section on the concept of quantum entanglement offers a qualitative validation of the method. The second chapter starts with a review of matrix product states. The theory of DMRG quantum chemical electronic structure calculations is analyzed using MPS. The final chapter presents the results of DMRG and CI calculations of t-PA systems.

Contents

Chapter 1

Introduction

In this chapter, the concept of correlation and different methods employed to account for different types of correlation are discussed first. A brief history of the DMRG method originally developed by White for solving one dimensional spin lattice systems follows. The chapter concludes with a short review of entanglement in quantum states and its quantitative measures. Validity of DMRG is explained using the area laws of entanglement entropy is presented.

1.1 Correlation in multi electronic systems

Correlation energy is defined as

$$E_{corr} = E_{exact} - E_{HF} \tag{1.1}$$

where, E_{exact} is the exact non relativistic ground state energy of the system and E_{HF} is the limit of the Hartree-Fock ground state energy as the number of basis functions tends to infinity (making a complete basis). The Hartree-Fock theory is based on the assumption of a single determinant electronic wavefunction. For systems in which the correlation is weak, results of the Hartree-Fock and other single reference theories agree reasonably with experiments. Thus the term correlation is used to describe the inadequacies of these theories. There are two ways in which the Hartree-Fock theory fails to account for electronic correlation. First, as a mean field theory it treats the Coulomb repulsion between electrons in an average way. Thus in a Hartree-Fock wavefunction, two electrons with opposite spins can be found at the same position in space with a nonzero probability i.e. there is no Coulomb hole. In reality the electrons avoid each other, thus leading to a more stable and lower energy system. The Hartree-Fock theory accounts for only a part of the correlation between electrons with parallel spins through the inclusion

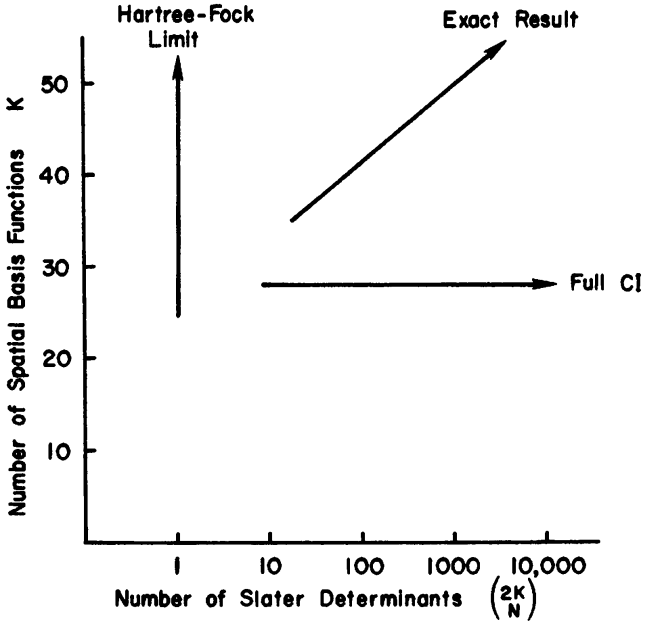

Figure 1.1: Limiting behavior of HF and FCI calculations [12]

of exchange interaction, as signified by the presence of the Fermi hole. This type of correlation is known as the dynamic correlation.

Dynamic correlation does not represent the complete picture though. Given the nature of dynamic correlation one would expect it to decrease at stretched geometries. However, experimentally it is observed that the correlation energy increases at stretched geometries. This is attributed to a different kind of correlation known as static correlation. Consider the Hartree-Fock treatment of hydrogen molecule in the minimal basis set. In the ground state both the electrons reside in the bonding σ orbital and the energy is given by $2h_{\sigma\sigma} + J_{\sigma\sigma}$. But as the internuclear distance tends to infinity, the ground state energy should approach $2h_{\sigma\sigma}$. Thus the HF theory overestimates the energy by $J_{\sigma\sigma}$. It can be seen that σ and σ_* orbitals become nearly degenerate for long internuclear distances. The HF theory assumes dominant contribution to the ground state wavefunction from a single determinant, while at stretched geometries (in H_2) the σ^2 and σ_*^2 become nearly degenerate and both contribute significantly to the ground state. This is true in general whenever the underlying states are nearly degenerate.

A way to remedy this is to consider multireference wavefunctions. One of the approaches of this kind is the well known configuration interaction method (CI). In Full CI the following wavefunction ansatz, constructed using

'excited' determinants derived from the HF ground state is considered,

$$|\Phi_0\rangle = c_0|\psi_0\rangle + \sum_{ar} c_a^r|\Psi_a^r\rangle + \sum_{a<b,r<s} c_{ab}^{rs}|\Psi_{ab}^{rs}\rangle + ... \tag{1.2}$$

The Hamiltonian is then diagonalized in the basis consisting of the ground state and all the excited determinants. Symmetry considerations notwithstanding, the total number of n-tuply excited determinants is $\binom{N}{n}\binom{2K-N}{n}$ (where $2K$ is the number of one electron spin orbitals and N is the number of electrons). This is an extremely large number even for small systems with modest basis sets. Thus truncations are made to the expansion by restricting the number of excitations giving rise to approximate methods like doubly excited CI, quadrupole CI, etc. In some methods a subset of orbitals (active space) forming the dominant states are first optimized and then CI is used on these states.

This discussion brings forth the major issue at the core of electronic structure calculation. The Hilbert space grows exponentially with the number of electrons making it very hard to get exact results as system size increases. As we will see in the upcoming chapter density matrix renormaliztion tackles this problem head on and provides a viable technique to accurately calculate the electronic structure of large systems (up to 40 electrons).

1.2 Historical development of DMRG: Spin lattice systems

Before getting into the details of DMRG quantum chemical calculation, we will briefly look at the historical development of the subject.

DMRG was introduced in 1992 by Steve White, as a numerical method to study one-dimensional quantum lattices[13][14], in light of the failure of Wilson's numerical renormalization group for strongly correlated systems. Consider a linear chain of L spins, with s=1/2, interacting via a local (interactions only with neighbors) Hamiltonian, say the Heisenberg Hamiltonian. Also assume open boundary conditions. We seek the ground state energy and wavefunction of this Hamiltonian. White proposed a two step procedure; starting with infinite-system DMRG followed by finite system DMRG. Note that the size of the Hilbert space grows as 2^L as the system size increases.

Infinite space DMRG overcomes the stumbling block of the exponentially growing Hilbert space by considering a chain of increasing length and systematically discarding a number of states to make the problem tractable.

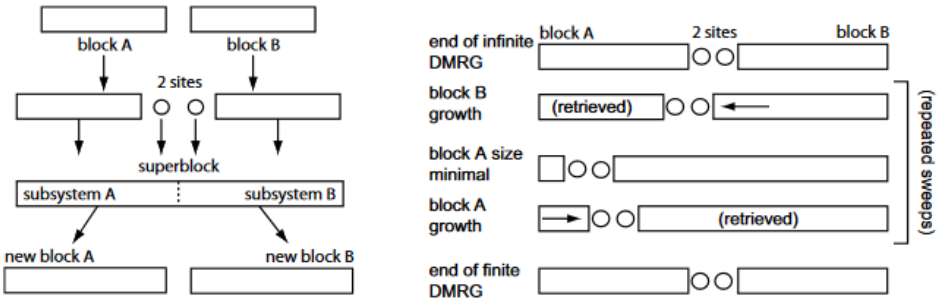

Figure 1.2: Pictorial representation of infinite (left) and finite (right) space DMRG
[9]

This procedure is based on the assumption that such a reduced space exists for local Hamiltonians, which we will justify in the next section. As the left panel of figure [1.2] illustrates, we start with two left and right blocks A and B of equal size (starting with one spin in each block, $L = 2$). Longer chains are built iteratively from the left and right end, by inserting pairs of spins between the blocks (the system grows as $L = 2,\ 4,\ 6, \dots$). The system always has a $A \bullet \bullet B$ structure. Let's assume that at any stage in the iteration, for block A we have an effective reduced Hilbert space with orthonormal basis $\{|a_l\rangle_A\}$, with dimension less than or equal to D (in practice D is of the order of 10^3 and the accuracy of the procedure relies on this value). For smaller blocks, the basis dimension would be less than D, for larger blocks some truncation must have occurred. Now we insert a pair of spins between the blocks and seek the ground state of this 'superblock'. This will also lead to bases for effective D-dimensional Hilbert spaces of $A\bullet$ and $\bullet B$. Any state of the superblock can be written as

$$|\psi\rangle = \sum_{a_A \sigma_a a_B \sigma_b} \psi_{a_A \sigma_a a_B \sigma_b} |a\rangle_A |\sigma\rangle_A |\sigma\rangle_B |a\rangle_B = \sum_{i_A j_B} \psi_{i_A j_B} |i\rangle_A |j\rangle_B \tag{1.3}$$

where the states of the newly introduced sites next between A and B are in the local 2 dimensional space spanned bu $|\sigma\rangle_A$ and $|\sigma\rangle_B$ respectively. The Hamiltonian is now diagonalized in this $4D^2$ dimensional space. In practice this is possible because the Hamiltonian matrix in this basis is sparse and can be efficiently diagonalized by algorithms given by Lanczos or Davidson.

$\{|i\rangle_A\}$ is a $2D$ dimensional basis for the block $A\bullet$. We need to truncate this to a D dimensional basis in order to avoid the exponential growth of the

Hilbert space. Reduced density matrix of a state is given by

$$[\rho_{A\bullet}]_{ii'} = \sum_j \psi_{ij}\psi^*_{i'j} \tag{1.4}$$

which is the partial trace of the density matrix of the composite $A \bullet \bullet B$ over $\bullet B$. This reduced matrix is now diagonalized and the eigenvectors corresponding to largest D eigenvalues are retained and made into an orthonormal basis for $A\bullet$. The basis for B is grown at the same time, for reflection-symmetric systems by simple mirroring. The rationale behind this procedure will be explained in the next section.

The operators also need to be expressed in the truncated basis and are updated in each iteration as

$$\langle a_l|\hat{O}|a'_l\rangle = \sum_{a_{l-1}\sigma_l\sigma'_l} \langle a_l|a_{l-1}\sigma_l\rangle\langle\sigma_l|\hat{O}|\sigma'_l\rangle\langle a_{l-1}\sigma'_l|a'_l\rangle \tag{1.5}$$

where, $\hat{O}$ is an operator acting on site l, which we assume is added to the left block A as its size increases from $l-1$ to l, $|a_l\rangle$ and $|a_{l-1}\rangle$ are basis sets of blocks of length l and $l-1$ respectively.

This iterative procedure is continued, until the desired system length is reached. Now the second step of the process, finite system DMRG, illustrated in the right panel of figure 1.2, is applied. This is very similar to the infinite system process, one of the blocks grows in the same way as before, but now at the expense of the other block, which shrinks in size. The Hamiltonian is diagonalized and basis set is truncated at each step as before. Growth in one direction continues until the shrinking block is reduced to one spin and then the sweep direction is reversed. This process is continued until energy converges. This is then the ground state energy of the system. .

1.3 Quantum Entanglement

In this section, we will justify the method outlined in the last section using the concept of quantum entanglement. First some terminology widely used in the field of quantum computation is introduced.

The density operator formulation is a useful tool for describing quantum systems whose state is not completely known, particularly subsystems of composite systems. Consider a system in one of the states $\{|\psi_i\rangle\}$, with probabilities p_i. This is called an ensemble of pure states (also known as mixed states). The density operator for the system is defined as

$$\rho = \sum_i p_i|\psi_i\rangle\langle\psi_i| \tag{1.6}$$

Note that for a pure state the ensemble contains only one state with probability one and the corresponding density operator is the projector onto the state. The Hilbert space of a composite system is given by the tensor product of the Hilbert spaces of constituents. Let's consider a bipartite system C made up of subsystems A and B. Then

$$\mathcal{H}_c = \mathcal{H}_A \otimes \mathcal{H}_B \tag{1.7}$$

A pure state $|\psi\rangle$[1] of the system C is said to be separable if it can be written as

$$|\psi\rangle = |\psi_A\rangle \otimes |\psi_B\rangle \tag{1.8}$$

A state entangled if and only if it is not separable. If ρ describes the state of system C then the reduced density matrix for system A is defined by

$$\rho_A = tr_B(\rho) \tag{1.9}$$

where tr_B is the partial trace over system B. If ρ corresponds to the state $|\psi\rangle = \sum_{ij} \Psi_{ij}|i\rangle_A|j\rangle_B$, thinking of Ψ_{ij} as entries of matrix Ψ, the reduced density matrices can be expressed as

$$\rho_A = \Psi\Psi^\dagger \qquad \rho_b = \Psi^\dagger\Psi \tag{1.10}$$

1.3.1 Schmidt decomposition

Singular value decomposition (SVD) is an extensively used tool in linear algebra, which will be very useful in introducing matrix product states. Here we use it to prove the Schmidt decomposition theorem.

Unfortunately there are many different but equivalent ways of formulating SVD in linear algebra literature. We will follow the one used in [3].

Theorem (SVD)**.** *If $A \in M_{m,n}$, has rank r, then it may be written in the form*

$$A = V\Sigma W^*$$

where $V \in M_m$ and $W \in M_n$ are unitary. The matrix $\Sigma = [\sigma_{ij}] \in M_{m,n}$ has $\sigma_{ij} = 0\ \forall i \neq j$ and $\sigma_{11} \geq \sigma_{22} \cdots \geq \sigma_{rr} > \sigma_{r+1,r+1} = \cdots = \sigma_{qq} = 0$ where $q = min\{m, n\}$ the numbers $\{\sigma_{ii} = \sigma_i\}$ are the nonnegative square roots of the eigenvalues of AA^*, and hence are uniquely determined. The columns of V are eigenvectors of AA^* and the columns of W are eigenvectors of A^*A. If A is real, then V, Σ and W may all be taken to be real.

[1] From here onwards a quantum state is assumed to be pure unless stated otherwise.

The proof uses the fact that matrices AA^* and A^*A are symmetric and proceeds by applying spectral theorem to these matrices.

Theorem (Schmidt decomposition[4]). *Suppose $|\psi\rangle$ is a pure state of a composite system AB. Then there exist orthonormal states $|a\rangle_A$ for system A and orthonormal states $|a\rangle_B$ for system B such that*

$$|\psi\rangle = \sum_a \lambda_a |a\rangle_A |a\rangle_B \tag{1.11}$$

The Schmidt decomposition theorem follows by applying SVD to matrix Ψ with entries given by, $|\psi\rangle = \sum_{ij} \Psi_{ij} |i\rangle_A |j\rangle_B$.

$$\begin{aligned}
|\psi\rangle &= \sum_{ij} \sum_a V_{ia} S_{aa} W^*_{ja} |i\rangle_A |j\rangle_B \\
&= \sum_a \left(\sum_i V_{ia} |i\rangle_A \right) s_a \left(\sum_j V^*_{ja} |j\rangle_B \right) \\
&= \sum_a s_a |a\rangle_A |a\rangle_B
\end{aligned}$$

Note that from SVD it follows that the reduced density matrices ρ_A and ρ_B have eigenvalues $s_a^2 = \lambda_a^2$ with eigenvectors $|a\rangle_A$ and $|a\rangle_B$. It can be easily seen that $r = 1$ for product states and $r > 1$ for entangled states.

The von Neumann entropy of a density matrix ρ is given by

$$S(\rho) = -tr(\rho ln \rho) = -\eta_i ln \eta_i \tag{1.12}$$

where η_i are the eigenvalues of ρ. Note that this is an extension of the Gibbs entropy to quantum systems. Since for a pure state ρ is idempotent $S(\rho)$ vanishes. Thus entropy quantifies the departure of the system from a pure state i.e. it quantifies the degree of mixing. For a state, represented using Schmidt decomposition as $|\psi\rangle = \sum_a s_a |a\rangle_A |a\rangle_B$, its entropy of entanglement is defined by

$$E(\psi) = S(\rho_A) = S(\rho_B) = -\sum_{a=1}^{r} s_a^2 ln s_a^2 \tag{1.13}$$

Therefore, two subsystems that partition a pure state are entangled if and only if their reduced states are mixed.

We conclude this section by mentioning one more applications of SVD. SVD can be used to minimize $\| D - \hat{D} \|_F$ over $\hat{D}$, subject to $rank(\hat{D}) \leq k$. Here D (rank r) and $\hat{D}$ are in $M_{m,n}$. $\|\|_F$ is the Frobenius norm. $\hat{D}$ is said to be a rank k approximation of D. Let's denote the SVD of D by

$D = V\Sigma W^*$. Now for any matrix $A \in M_{m,n}$ define the matrix $D' = V^*AW$, so $A = VD'W^*$. Then

$$\| D - A \|_F^2 = \| \Sigma - D' \|_F^2 \geq \sum_{i>k} |\sigma_i - D'_{ii}|^2 \tag{1.14}$$

Thus the rank k approximation of D is given by $\hat{D}$ with nonzero diagonal entries $(\sigma_1, \ldots, \sigma_k)$.

The 2-norm of the state $|\psi\rangle$ defined above is equal to the Frobenious norm of the corresponding coefficient matrix Ψ. Thus the best rank k approximation of the state $|\psi\rangle$, say $|\tilde{\psi}\rangle$, is given by the state

$$|\tilde{\psi}\rangle = \sum_{a=1}^{k} s_a |a\rangle_A |a\rangle_B \tag{1.15}$$

This sheds some light on the truncation procedure used in DMRG. Note that the accuracy of the approximation depends on how rapidly the spectrum of eigenvalues decays.

1.3.2 Justifying DMRG: Quantum information perspective

If we know the spectrum of the reduced density matrices we can gauge the accuracy of the truncation procedure employed in DMRG. Analysis of some exactly solvable systems suggests that the spectrum decays rapidly for one dimensional systems with gapped Hamiltonians. But in general no prediction can be made about the spectrum of eigenvalues.

But all is not lost, as entanglement encodes the vital information about the spectrum and scaling laws of entanglement entropies, known as area laws, are available. For a bipartite system $A|B$, with A of size L^D (D: spatial dimension), the area laws predict that for ground states of local gapped Hamiltonians the entropy of entanglement is proportional to the area of the boundary between A and B i.e. $S(A|B) \sim L^{D-1}$ (away from criticality and in thermodynamic limit) 1.3. Thus entanglement is not an extensive quantity (not proportional to volume). In one dimension, $S \sim constant$. Maximal entanglement between two systems of dimension D is lnD. As S doesn't change with system size for such systems, D can be kept constant even as the system size increases. Note that in two dimensions, $S \sim 2^L$, so DMRG fails for even small systems in two dimensions. Essence of this discussion is that although the size of the Hilbert space grows exponentially with system size, for local gapped Hamiltonians, the ground state is restricted to a small region

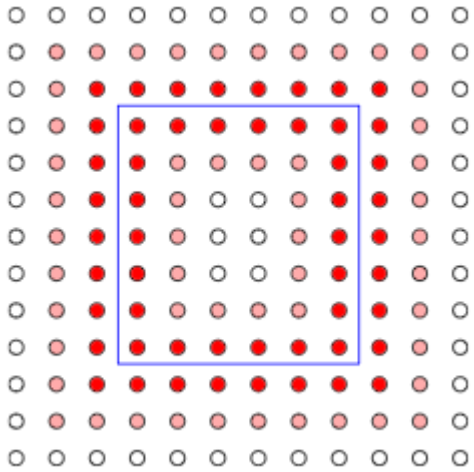

Figure 1.3: Illustration of the area law

in the Hilbert space. This is the region targeted by the DMRG algorithm, as we will see in the next chapter.

Chapter 2

DMRG using Matrix Product States

In the last chapter we saw the successes of DMRG in calculating ground states of spin lattice systems. It was soon realized after the discovery of DMRG that it can be applied to solving quantum chemical electronic structure problems. White proposed a way to do ab initio electronic structure calculation using DMRG in 1999 [15]. This formulation of DMRG primarily used the same framework described in the last chapter. However, as is now understood, the DMRG algorithm minimises the energy of a wavefunction ansatz known as the matrix product state (MPS) [7]. MPSs are generalizations of simple product states. They provide flexibility in representing and approximating states with different amounts of entanglement. In this chapter we will first develop the theory of matrix product states. Then we will see how DMRG is applied to calculate electronic structure using MPSs.

2.1 Matrix product states

Although the Hilbert space of a quantum system exponentially with size, the ground states of local gapped Hamiltonians are heavily constrained by the entanglement entropy area laws and do not span the whole space. It seems logical then, to focus on this small part of the space rather than searching through the whole Hilbert space. Matrix product states prove to be the best tool for targeting the relevant part of the space. Instead of starting with the definition of a MPS we will prescribe a procedure to construct one from a general quantum state. We turn our attention from spin systems to quantum chemical electronic systems which are more relevant to the discussion in this chapter. Hamiltonian of a multi-electron system can be written as[16]

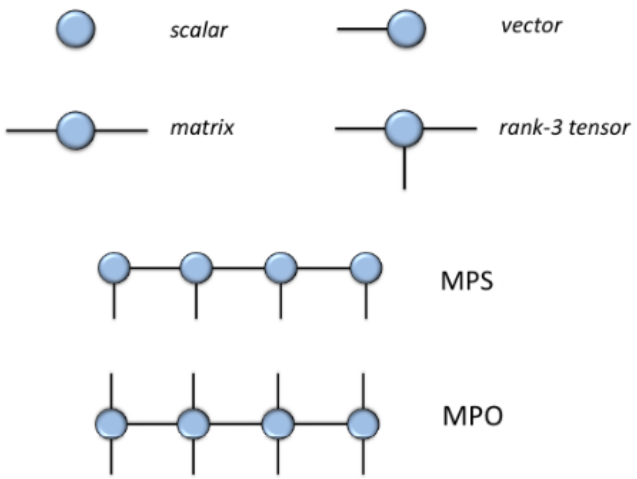

Figure 2.1: Tensor network diagrams[6]

$$\hat{H} = E_0 + \sum_{ij} t_{ij} \sum_{\sigma} \hat{a}^{\dagger}_{i\sigma} \hat{a}_{j\sigma} + \frac{1}{2} \sum_{ijkl} v_{ij,kl} \sum_{\sigma\tau} \hat{a}^{\dagger}_{i\sigma} \hat{a}^{\dagger}_{j\tau} \hat{a}_{l\tau} \hat{a}_{k\sigma} \tag{2.1}$$

where the Latin indices denote spatial orbitals while Greek indices electronic spin. If we restrict to L basis orbitals in the one particle Hilbert space, a general state of the multi-electron system can be written in the occupation number representation as

$$|\psi\rangle = \sum_{n_{j\sigma}} C_{n_{1\uparrow} n_{1\downarrow} \ldots n_{L\uparrow} n_{L\downarrow}} |n_{1\uparrow} n_{1\downarrow} \ldots n_{L\uparrow} n_{L\downarrow}\rangle \tag{2.2}$$

The correspondence between this representation of the electronic system and the system of spins studied in the last chapter is apparent. We can assume the orbitals to be placed on a one-dimensional lattice. The expansion coefficients can be realized as entries of a tensor, which can be reshaped into a matrix Ψ of dimension $4 \times 4^{L-1}$as

$$\Psi_{(n_{1\uparrow} n_{1\downarrow});(n_{2\uparrow} n_{2\downarrow} \ldots n_{L\uparrow} n_{L\downarrow})} = C_{n_{1\uparrow} n_{1\downarrow} \ldots n_{L\uparrow} n_{L\downarrow}} \tag{2.3}$$

Now SVD of Ψ gives

$$\Psi_{(n_{1\uparrow} n_{1\downarrow});(n_{2\uparrow} n_{2\downarrow} \ldots n_{L\uparrow} n_{L\downarrow})} = \sum_{\alpha_1}^{r_1} U[1]_{n_{1\uparrow} n_{1\downarrow};\alpha_1} s[1]_{\alpha 1} V[1]_{\alpha_1; n_{2\uparrow} n_{2\downarrow} \ldots n_{L\uparrow} n_{L\downarrow}} \tag{2.4}$$

Define

$$A[1]^{n_{1\uparrow}n_{1\downarrow}}_{\alpha_1} = U[1]_{n_{1\uparrow}n_{1\downarrow};\alpha_1} s[1]_{\alpha 1} \tag{2.5}$$

Note that this step associates 4 vectors viz. $A[1]^{n_{1\uparrow}n_{1\downarrow}}_{\alpha_1}$, of length r_1 to the first site. Reshape $V[1]$ into a matrix Ψ of dimension $4r_1 \times 4^{L-2}$, to give

$$C_{n_{1\uparrow}n_{1\downarrow}\ldots n_{L\uparrow}n_{L\downarrow}} = \sum_{\alpha_1}^{r_1} A[1]^{n_{1\uparrow}n_{1\downarrow}}_{\alpha_1} \Psi_{(\alpha_1 n_{2\uparrow}n_{2\downarrow});(n_{3\uparrow}n_{3\downarrow}\ldots n_{L\uparrow}n_{L\downarrow})} \tag{2.6}$$

SVD is again applied to Ψ, to get

$$\Psi_{(\alpha_1 n_{2\uparrow}n_{2\downarrow});(n_{3\uparrow}n_{3\downarrow}\ldots n_{L\uparrow}n_{L\downarrow})} = \sum_{\alpha_2}^{r_2} U[2]_{\alpha_1 n_{2\uparrow}n_{2\downarrow};\alpha_2} s[2]_{\alpha_2} V[2]_{\alpha_2;n_{3\uparrow}n_{3\downarrow}\ldots n_{L\uparrow}n_{L\downarrow}} \tag{2.7}$$

Define

$$A[2]^{n_{2\uparrow}n_{2\downarrow}}_{\alpha_1;\alpha_2} = U[2]_{\alpha_1 n_{2\uparrow}n_{2\downarrow};\alpha_2} s[2]_{\alpha_2} \tag{2.8}$$

So that

$$C_{n_{1\uparrow}n_{1\downarrow}\ldots n_{L\uparrow}n_{L\downarrow}} = \sum_{\alpha_1}^{r_1}\sum_{\alpha_2}^{r_2} A[1]^{n_{1\uparrow}n_{1\downarrow}}_{\alpha_1} A[2]^{n_{2\uparrow}n_{2\downarrow}}_{\alpha_1;\alpha_2} \Psi_{(\alpha_2 n_{3\uparrow}n_{3\downarrow});(n_{4\uparrow}n_{4\downarrow}\ldots n_{L\uparrow}n_{L\downarrow})} \tag{2.9}$$

Note that this step associates four matrices viz. $A[2]^{n_{2\uparrow}n_{2\downarrow}}_{\alpha_1;\alpha_2}$ of dimensions $r_1 \times r_2$ to the second site. Continuing this procedure we eventually get the following contracted matrix product,

$$C_{n_{1\uparrow}n_{1\downarrow}\ldots n_{L\uparrow}n_{L\downarrow}} = \sum_{\alpha_1,\ldots,\alpha_{L-1}} A[1]^{n_{1\uparrow}n_{1\downarrow}}_{\alpha_1} A[2]^{n_{2\uparrow}n_{2\downarrow}}_{\alpha_1;\alpha_2} \ldots A[2]^{n_{L\uparrow}n_{L\downarrow}}_{\alpha_{L-1}} \tag{2.10}$$

This represents a MPS with open boundary conditions. The superscripts $n_{i\uparrow}n_{i\downarrow}$ are called physical indices, while the subscripts α_{i-1} and α_i virtual indices. In fig. 2.1, open lines represent physical indices while the connected lines denote the contracted virtual indices. The virtual state spaces may be visualized to be associated with the bonds $(i, i+1)$ and $(i-1, i)$. The matrices at each site map between neighboring virtual spaces.

It should be noted that the matrix product representation of state is not unique. A gauge degree of freedom exists in the choice of $A[i]$. Consider two adjacent sets of matrices $A[i]$ and $A[i+1]$ of shared dimension D. Then the MPS is invariant under the transformation

$$A[i] \to A[i]X, \qquad A[i+1] \to X^{-1}A[i+1] \tag{2.11}$$

where X is of dimension $D \times D$. The procedure used above to arrive at the MPS implicitly makes a gauge choice. The matrices $A[i]$ above satisfy the condition

$$\sum_{n_{i\uparrow} n_{i\downarrow}} A[i]^{n_{i\uparrow} n_{i\downarrow}\dagger} A[i]^{n_{i\uparrow} n_{i\downarrow}} = I \tag{2.12}$$

These matrices are said to be left-normalized and MPSs made up of left-normalized matrices are said to be left-canonical. In an exactly analogous way we can start from the last site and obtain a right-canonical MPS made up of right-normalized matrices, which satisfy the condition

$$\sum_{n_{i\uparrow} n_{i\downarrow}} B[i]^{n_{i\uparrow} n_{i\downarrow}} B[i]^{n_{i\uparrow} n_{i\downarrow}\dagger} = I \tag{2.13}$$

In the DMRG procedure we will be using what are known as mixed-canonical MPSs, with coefficients given by

$$C_{n_{1\uparrow} n_{1\downarrow} \ldots n_{L\uparrow} n_{L\downarrow}} = A[1]^{n_{1\uparrow} n_{1\downarrow}} \ldots A[l]^{n_{l\uparrow} n_{l\downarrow}} SB[l+1]^{n_{l+1\uparrow} n_{l+1\downarrow}} \ldots B[L]^{n_{L\uparrow} n_{L\downarrow}} \tag{2.14}$$

where $A[i]$ are left-normalized and $B[i]$ are right-normalized.

A natural generalization of this representation can be made to operators (matrix product operators).

$$\hat{O} = \sum_{\mathbf{n},\mathbf{n'}} W^{n_1 n'_1} W^{n_2 n'_2} \ldots W^{n_L n'_L} |\mathbf{n}\rangle\langle\mathbf{n'}| \tag{2.15}$$

where $|\mathbf{n}\rangle$ and $|\mathbf{n'}\rangle$ are basis states. Two spin indices have been contracted into a single one which can take four values 2.1.

2.2 DMRG and MPS

Having formally introduced MPSs we are now ready to use them for DMRG calculations. Before analyzing the full algorithm for ground state calculation we will first try to understand the connection between MPSs and DMRG.

Suppose that we have reached a stage in the iterative DMRG algorithm where the left block is of size $l-1$ and we have an effective D-dimensional basis $\{|a_{l-1}\rangle_A\}$ on this block. When increasing the size from $l-1$ to l, the dimension of the new system is truncated to a constant D if necessary, to avoid exponential growth of the Hilbert space. If the new basis after truncation is $\{|a_l\rangle_A\}$, we have

$$|a_l\rangle_A = \sum_{a_{l-1} n_l} {}_A\langle a_{l-1} n_l | a_l\rangle_A |a_{l-1}\rangle_A |n_l\rangle \tag{2.16}$$

where $|n_l\rangle$ are the basis states at the site l. Define

$$A^{n_l}_{a_{l-1}a_l} =_A \langle a_{l-1} n_l | a_l \rangle_A \tag{2.17}$$

Recursing this procedure leads to

$$|a_l\rangle_A = \sum_{n_l \in A} (A^{n_1} A^{n_2} \dots A^{n_l})_{1,a_l} |n_1 n_2 \dots n_l\rangle \tag{2.18}$$

Thus we see that the states resulting from truncation in DMRG are naturally expressed as $D \times D$ matrix product states[7]. DMRG actually finds the MPS that minimizes ground state energy.

For a general state the maximal dimensions of the matrices making up the matrix product representation can be counted as $1 \times 4,\ 4 \times 4^2, \dots,\ 4^{L/2-1} \times 4^{L/2},\ 4^{L/2} \times 4^{L/2-1} \dots, 4 \times 1$ going from the first to the last site. As expected we see that the sizes of the matrices increase exponentially with L. In DMRG, as seen above, the dimension is capped by D at each stage.

$$dim(\alpha_j) = min(4^j, 4^{L-j}, D) \tag{2.19}$$

Thus the maximum number of variables is LdD^2. Note that the number of variables scales linearly with system size.

It can be shown that for a bipartite MPS (with virtual dimension capped by D), say $X|Y$, the entanglement entropy satisfies $S(\rho_x) \leq log(D)$. If the targeted state also satisfies this condition for all partitions then it can be written in the MPS from of virtual dimension D. We know from last chapter that this is indeed the case for ground states of one-dimensional local gapped Hamiltonians.

2.2.1 Variational optimization

Now we will discuss the two-site DMRG algorithm wherein at each iteration two neighboring sites are simultaneously optimized.

$$\sum_{\alpha_i} A[i]^{n_i}_{\alpha_{i-1};\alpha_i} A[i+1]^{n_{i+1}}_{\alpha_i;\alpha_{i+1}} = C[i]^{n_i;n_{i+1}}_{\alpha_{i-1};\alpha_{i+1}} \tag{2.20}$$

It is insured that matrices on the left of the pair being optimized are left-normalized while those on the right are right-normalized. Minimizing

$$\mathcal{L} = \langle \Psi(C[i]) | \hat{H} | \Psi(C[i]) \rangle - \lambda \langle \Psi(C[i]) | \Psi(C[i]) \rangle \tag{2.21}$$

with respect to $C[i]$, we get[1]

$$\mathbf{H}^{eff} C[i] = \lambda C[i] \tag{2.22}$$

After the lowest eigenvalue and eigenvector are found, $C[i]$ decomposed with SVD,

$$C[i]_{(\alpha_{i-1}n_i);(n_{i+1}\alpha_{i+1})} = \sum_{\beta} U[i]_{(\alpha_{i-1}n_i);\beta} s[i]_{\beta} V[i]_{\beta;(n_{i+1}\alpha_{i+1})} \tag{2.23}$$

where $U[i]$ is left-normalized and $V[i]$ is right normalized. β is truncated to D at each iteration. This optimization of a pair of matrices is called a micro-iteration. The system is sweeped from left to right with micro-iterations at each site. The direction of sweeping is reversed when the process reaches the rightmost site. This process is continued until the energy converges. The choice of D and ordering of the orbitals has a significant effect on the rate of convergence. The orbitals should be ordered so that the correlation length is minimized. Determining the optimal ordering is a topic of ongoing research.

Chapter 3

Application of DMRG to polyenes

In this chapter I will present the results of the DMRG calculations of ground and low lying excited states of all-trans polyenes (also known as trans polyacetylene or t-PA) up to $C_{18}H_{20}$ (t-PA9) and compare them with FCI results. The Pariser-Parr-Pople (PPP) model Hamiltonian was used to get the single electron orbitals and energies. We start with a brief review of PPP model Hamiltonian.

3.1 Pariser-Parr-Pople (PPP) Hamiltonian

Pariser, Parr and Pople proposed a model Hamiltonian for π-conjugated systems in 1950's. The PPP Hamiltonian can be written as[11]

$$H_{PPP} = \sum_{i,\sigma} \epsilon_i c^\dagger_{i\sigma} c_{i\sigma} + \sum_{<ij>,\sigma} t_{ij}(c^\dagger_{i\sigma} c_{j\sigma} + c^\dagger_{j\sigma} c_{i\sigma}) + U \sum_i n_{i\uparrow} n_{i\downarrow} + \sum_{i<j} V_{ij}(n_i - 1)(n_j - 1) \tag{3.1}$$

where ϵ_i is the site energy, which is the energy of π orbital at i, $c^\dagger_{i\sigma}$ creates an electron with spin σ in the p_z orbital of carbon atom at site i. $n_{i\sigma}$ is the number operator at site i. U and V_{ij} are the on-site and long-range Coulomb interactions, respectively. t_{ij} are the nearest-neighbor hopping terms ($< ij >$ denotes nearest neighbor). These represent the kinetic energy of the electrons. Note that this Hamiltonian reduces to the Hubbard model if the long-range interactions V_{ij} are neglected. This Hamiltonian can be diagonalized in the basis set of the p_z orbitals of all the carbon atoms using the Pople-Nesbet equations.

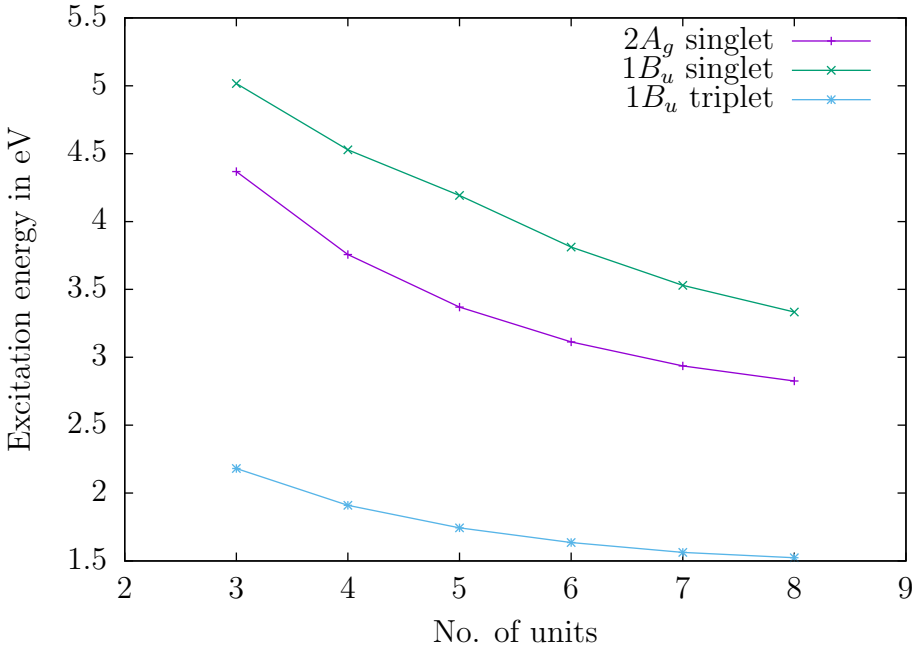

Figure 3.1: Excitation energies

3.2 Results of t-PA calculations

The PPP RHF calculations were done using a `FORTRAN 90` program written by Alok Shukla et.al.[11]. We used the free open source `C++` program `CheMPS2`, a spin adapted implementation of DMRG, developed by Sebastian Wouters et.al.[17]. The `MELD` package was used for CI calculations. Following tables show the QCI, FCI (only up to t-PA4) and DMRG energies calculated for the ground and first two excited states of both singlet and triplet. All the energies are in eV. The DMRG energies compare well with FCI energies. To ensure fast convergence and to avoid trapping in local minima, a sequence of calculations was done with increasing values of D. The energies reported below correspond to the final calculation of the sequence, with $D = 1000$.[1]

[1]It should be noted that the energy extrapolation to $D \to \infty$ was not used, in order to compare true variational DMRG and CI energies.

Polyene	State	QCI	FCI	DMRG
$t-PA3$	$^1A_g1$	-12.458342725	-12.458779869	-12.458779869125
	$^1A_g2$	-8.0907535920	-8.0908455938	-8.090845604276
	$^1A_g3$	-5.7328626978	-5.7385345880	-5.738534573690
	$^1B_u1$	-7.4422498338	-7.4422498338	-7.442249853749
	$^1B_u2$	-7.1102846087	-7.1102846087	-7.110284719014
	$^1B_u3$	-4.8922607189	-4.8922607189	-4.892260756668
	$^3B_u1$	-10.2775441986	-10.2775441986	-10.277544235651
	$^3B_u2$	-8.0902898177	-8.0902898177	-8.090289796288
	$^3B_u3$	-6.9325481133	-6.9325481133	-6.932548125076
$t-PA4$	$^1A_g1$	-16.8705045352	-16.872654897	-16.872654893347
	$^1A_g2$	-13.0980180280	-13.1152751303	-13.115275153012
	$^1A_g3$	-11.5287037281	-11.5418352844	-11.541835186370
	$^1B_u1$	-12.3442194268	-12.3447199161	-12.344719931298
	$^1B_u2$	-12.1580393892	-12.1656494667	-12.165649459403
	$^1B_u3$	-10.2133324821	-10.2290160254	-10.229016052787
	$^3B_u1$	-14.9617650290	-14.9632965985	-14.963296643552
	$^3B_u2$	-13.0200987978	-13.0246444423	-13.024644378794
	$^3B_u3$	-12.1165034330	-12.1233346617	-12.123334659033
$t-PA5$	$^1A_g1$	-21.282936759	-21.288916309	-21.288916292248
	$^1A_g2$	-17.864130366	-17.918799369	-17.918799384077
	$^1A_g3$	-16.350407173	-16.396745852	-16.396745788914
	$^1B_u1$	-17.087379681	-17.089770393	-17.096594094613
	$^1B_u2$	-17.069784738	-17.096317220	-17.090463702028
	$^1B_u3$	-15.938079246	-15.972423601	-15.972833470726
	$^3B_u1$	-19.535982214	-19.542952522	-19.545396777145
	$^3B_u2$	-17.881574827	-17.898719490	-17.900647569262
	$^3B_u3$	-17.041954408	-17.067469525	-17.068310442816
$t-PA6$	$^1A_g1$	-25.69344852	-25.705486655	-25.70602063
	$^1A_g2$	-22.480491045	-22.590983944	-22.59292766
	$^1A_g3$	-21.147127180	-21.238519757	-21.24117143
	$^1B_u1$	-21.833260854	-21.891733830	-21.89397587
	$^1B_u2$	-21.731337291	-21.737851108	-21.74130324
	$^1B_u3$	-20.618218449	-20.698202264	-20.70178899
	$^3B_u1$	-24.044655515	-24.062527620	-24.07072971
	$^3B_u2$	-22.633732095	-22.672557636	-22.68021800
	$^3B_u3$	-21.790799685	-21.849482995	-21.85449799

$t-PA7$	$^1A_g1$	-30.10108	-30.12101	-30.12338
	$^1A_g2$	-26.999350	-27.177630	-27.186590
	$^1A_g3$	-25.143774	-25.999530	-26.009520
	$^1B_u1$	-26.48034	-26.58212	-26.59301
	$^1B_u2$	-26.30755	-26.32095	-26.33067
	$^1B_u3$	-25.33062	-25.45955	-25.47265
	$^3B_u1$	-28.50765	-28.54190	-28.56034
	$^3B_u2$	-27.29145	-27.35961	-27.37677
	$^3B_u3$	-26.41500	-26.52003	-26.52969
$t-PA8$	$^1A_g1$	-34.50537		-34.53892
	$^1A_g2$	-31.452610		-31.71369
	$^1A_g3$	-30.477940		-30.68713
	$^1B_u1$	-31.03991		-31.20570
	$^1B_u2$	-30.83357	-	-30.87664
	$^1B_u3$	-29.98617		-30.18422
	$^3B_u1$	-32.93623		-33.01562
	$^3B_u2$	-31.87445		-31.99596
	$^3B_u3$	-30.94953		-31.10022
$t-PA9$	$^1A_g1$	-38.90604		-38.94919
	$^1A_g2$	-35.860710		-36.17336
	$^1A_g3$	-35.032670		-35.26702
	$^1B_u1$	-35.53143	-	-35.73227
	$^1B_u2$	-35.32079		-35.38718
	$^1B_u3$	-34.57614		-34.80684

Table 3.2: Calculated energies of t-PA singlet and triplet states

PPP-DMRG calculations with polyacenes, polyparaphenyl (also abbreviated PPP) and trigonal nanodisks were done using both screened and standard parameters in the summer following the BTech project. Methodology used was the similar to that for the t-PA calculations. Further details of these calculations will be reported in a publication soon.

Polyacenes

Acene	State	QCI	FCI	DMRG
$Acene-2\ (scr)$	$^1A_g1$	-21.231665	-21.245326	-21.245326
	$^1A_g2$	-16.778122	-16.879752	-16.879752
	$^1A_g3$	-16.132909	-16.230828	-16.230828
	$^1B_{3u}1$	-17.973619	-18.027494	-18.027494
	$^1B_{3u}2$	-15.914066	-15.945570	-15.945570
	$^1B_{3u}3$	-15.494116	-15.578208	-15.578207
	$^1B_{2u}1$	-16.725197	-16.731789	-16.733495
	$^1B_{2u}2$	-15.098515	-15.126994	-15.131767
	$^1B_{2u}3$	-14.552948	-14.685479	-14.689363
	$^1B_{1g}1$	-16.399262	-16.468476	-16.468475
	$^1B_{1g}2$	-15.383603	-15.496246	-15.496246
	$^1B_{1g}3$	-14.852170	-14.879300	-14.879300
	$^3B_{3u}1$	-17.876041	-17.917925	-17.917925
	$^3B_{3u}2$	-16.442217	-16.462533	-16.462533
	$^3B_{3u}3$	-15.952453	-16.037961	-16.037961
	$^3B_{2u}1$	-19.118211	-19.132710	-19.140764
	$^3B_{2u}2$	-17.429214	-17.477969	-17.491411
	$^3B_{2u}3$	-15.625677	-15.689570	-15.696835
	$^3B_{1g}1$	-17.926667	-17.969360	-17.969360
	$^3B_{1g}2$	-16.366059	-16.454480	-16.454480
	$^3B_{1g}3$	-15.608042	-15.631783	-15.631782

Table 3.3: Acene 2 screened

Acene	State	QCI	FCI	DMRG
$Acene-2\ (std)$	$^1A_g1$	-24.091644	-24.095718	-24.095718
	$^1A_g2$	-19.169754	-19.203886	-19.203886
	$^1A_g3$	-18.396669	-18.425356	-18.425356
	$^1B_{3u}1$	-20.471611	-20.484839	-20.484839
	$^1B_{3u}2$	-18.100980	-18.110086	-18.110086
	$^1B_{3u}3$	-17.785872	-17.811819	-17.811819
	$^1B_{2u}1$	-19.644644	-19.647236	-19.647470
	$^1B_{2u}2$	-17.989607	-17.995415	-17.996438
	$^1B_{2u}3$	-16.627363	-16.670660	-16.671862
	$^1B_{1g}1$	-18.724095	-18.747290	-18.747290
	$^1B_{1g}2$	-18.271346	-18.277974	-18.277974
	$^1B_{1g}3$	-17.479520	-17.523428	-17.523428
	$^3B_{3u}1$	-20.356551	-20.366031	-20.366031
	$^3B_{3u}2$	-19.331451	-19.335137	-19.335137
	$^3B_{3u}3$	-18.165555	-18.187670	-18.187670
	$^3B_{2u}1$	-21.561073	-21.565198	-21.567095
	$^3B_{2u}2$	-19.791947	-19.804155	-19.807521
	$^3B_{2u}3$	-17.820521	-17.836750	-17.838865
	$^3B_{1g}1$	-20.344651	-20.356674	-20.356674
	$^3B_{1g}2$	-18.627926	-18.655666	-18.655666
	$^3B_{1g}3$	-17.962789	-17.969055	-17.969055

Table 3.4: Acene 2 standard

Acene	State	QCI	FCI	DMRG
$Acene-3\ (scr)$	$^1A_g1$	-30.017779	-30.061883	-30.065992
	$^1A_g2$	-26.344622	-26.580694	-26.596829
	$^1A_g3$	-25.562375	-25.785483	-25.808448
	$^1B_{3u}1$	-26.995622	-27.152327	-27.180474
	$^1B_{3u}2$	-25.398134	-25.672074	-25.697101
	$^1B_{3u}3$	-25.301162	-25.415665	-25.431778
	$^1B_{2u}1$	-26.486676	-26.509510	-26.529015
	$^1B_{2u}2$	-25.408516	-25.559938	-25.587811
	$^1B_{2u}3$	-24.130369	-24.375672	-24.403091
	$^1B_{1g}1$	-26.045376	-26.196057	-26.217492
	$^1B_{1g}2$	-25.158381	-25.251164	-25.265467
	$^1B_{1g}3$	-24.201908	-24.543041	-24.573129
	$^3B_{3u}1$	-26.877354	-27.015887	-27.036801
	$^3B_{3u}2$	-25.668673	-25.782338	-25.807015
	$^3B_{3u}3$	-25.541910	-25.756962	-25.771278
	$^3B_{2u}1$	-28.542994	-28.581635	-28.624790
	$^3B_{2u}2$	-26.648252	-26.781800	-26.821836
	$^3B_{2u}3$	-26.014098	-26.182787	-26.244931
	$^3B_{1g}1$	-27.360119	-27.480001	-27.505489
	$^3B_{1g}2$	-25.461580	-25.714068	-25.744532
	$^3B_{1g}3$	-25.409716	-25.496690	-25.510171

Table 3.5: Acene 3 screened

Acene	State	QCI	FCI	DMRG
$Acene-3\ (std)$	$^1A_g1$	-33.969952	-33.985884	-33.987035
	$^1A_g2$	-29.990165	-30.097752	-30.103397
	$^1A_g3$	-28.910107	-29.011066	-29.019790
	$^1B_{3u}1$	-30.683392	-30.737773	-30.746781
	$^1B_{3u}2$	-28.978510	-29.087312	-29.095699
	$^1B_{3u}3$	-28.600876	-28.642372	-28.646600
	$^1B_{2u}1$	-30.314013	-30.326309	-30.330848
	$^1B_{2u}2$	-28.953764	-29.009430	-29.018437
	$^1B_{2u}3$	-28.249695	-28.280688	-28.288341
	$^1B_{1g}1$	-29.609817	-29.672212	-26.217492
	$^1B_{1g}2$	-29.151648	-29.184569	-25.265467
	$^1B_{1g}3$	-27.651668	-27.717532	-24.573129
	$^3B_{3u}1$	-30.533062	-30.578404	-30.585333
	$^3B_{3u}2$	-29.632707	-29.658581	-29.662281
	$^3B_{3u}3$	-29.024300	-29.108608	-29.118672
	$^3B_{2u}1$	-32.240745	-32.256256	-32.269389
	$^3B_{2u}2$	-30.273973	-30.318924	-30.332083
	$^3B_{2u}3$	-29.505684	-29.563884	-29.584404
	$^3B_{1g}1$	-30.988637	-31.034231	-31.042454
	$^3B_{1g}2$	-28.951647	-29.055489	-29.066312
	$^3B_{1g}3$	-28.919489	-28.952258	-28.955530

Table 3.6: Acene 3 standard

State	QCI	FCI	DMRG
$^1A_g1$	-38.748161	-	-38.767953
$^1A_g2$	-35.639580	-	-35.885093
$^1A_g3$	-34.826591	-	-34.993326
$^1B_{3u}1$	-35.772049	-	-35.969713
$^1B_{3u}2$	-34.774138	-	-35.059273
$^1B_{3u}3$	-34.305058	-	-34.494806
$^1B_{2u}1$	-35.778861	-	-35.812485
$^1B_{2u}2$	-34.579035	-	-34.748219
$^1B_{2u}3$	-33.635636	-	-33.753580
$^1B_{1g}1$	-35.344285	-	-35.501284
$^1B_{1g}2$	-34.584524	-	-34.697143
$^1B_{1g}3$	-34.106975	-	-34.336882
$^3B_{3u}1$	-35.687619	-	-35.720356
$^3B_{3u}2$	-34.962464	-	-35.172472
$^3B_{3u}3$	-34.566526	-	-34.661172
$^3B_{2u}1$	-37.637311	-	-37.681022
$^3B_{2u}2$	-35.721548	-	-35.830303
$^3B_{2u}3$	-34.689735	-	-34.760396
$^3B_{1g}1$	-36.575920	-	-36.654869
$^3B_{1g}2$	-35.223111	-	-35.350745
$^3B_{1g}3$	-34.817036	-	-34.894804

Table 3.7: Acene 4 screened

State	QCI	FCI	DMRG
$^1A_g1$	-43.803425	-	-43.819633
$^1A_g2$	-40.480116	-	-40.630868
$^1A_g3$	-39.508265	-	-39.605234
$^1B_{3u}1$	-40.644521	-	-40.741480
$^1B_{3u}2$	-39.628651	-	-39.770199
$^1B_{3u}3$	-38.804072	-	-38.883044
$^1B_{2u}1$	-40.645184	-	-40.664837
$^1B_{2u}2$	-39.328619	-	-39.404653
$^1B_{2u}3$	-38.767262	-	-38.812704
$^1B_{1g}1$	-40.111234	-	-40.202885
$^1B_{1g}2$	-39.629159	-	-39.676013
$^1B_{1g}3$	-38.885183	-	-39.003470
$^1B_{3u}1$	-40.518340	-	-40.540541
$^1B_{3u}2$	-39.700907	-	-39.696836
$^1B_{3u}3$	-39.654635	-	-39.804141
$^1B_{2u}1$	-42.548638	-	-42.568540
$^1B_{2u}2$	-40.553948	-	-40.594250
$^1B_{2u}3$	-39.306952	-	-39.338007
$^1B_{1g}1$	-41.443346	-	-41.483672
$^1B_{1g}2$	-40.070842	-	-40.126336
$^1B_{1g}3$	-39.480470	-	-39.516228

Table 3.8: Acene 4 standard

State	QCI	FCI	DMRG
$^1A_g1$	-47.439448	-	-47.348891
$^1A_g2$	-44.699563	-	-44.910479
$^1A_g3$	-43.786253	-	-43.820491
$^1B_{3u}1$	-44.418602	-	-44.466110
$^1B_{3u}2$	-43.895384	-	-44.053536
$^1B_{3u}3$	-43.085336	-	-43.261614
$^1B_{2u}1$	-44.793029	-	-44.850664
$^1B_{2u}2$	-43.625762	-	-43.612817
$^1B_{2u}3$	-42.810721	-	-42.849819
$^1B_{1g}1$	-44.378307	-	-44.385828
$^1B_{1g}2$	-43.706349	-	-43.800611
$^1B_{1g}3$	-42.958385	-	-42.990826
$^3B_{3u}1$	-44.495259	-	-44.458399
$^3B_{3u}2$	-43.962115	-	-43.922352
$^3B_{3u}3$	-43.279726	-	-43.364010
$^3B_{2u}1$	-46.509518	-	-46.496906
$^3B_{2u}2$	-44.741928	-	-44.685572
$^3B_{2u}3$	-43.804759	-	-43.694951
$^3B_{1g}1$	-45.572786	-	-45.520103
$^3B_{1g}2$	-44.053453	-	-43.928040
$^3B_{1g}3$	-43.911375	-	-44.020286

Table 3.9: Acene 5 screened

State	QCI	FCI	DMRG
$^1A_g1$	-53.613853	-	-53.580862
$^1A_g2$	-50.726761	-	-50.774226
$^1A_g3$	-49.776017	-	-49.685725
$^1B_{3u}1$	-50.471239	-	-50.541516
$^1B_{3u}2$	-49.985687	-	-50.110487
$^1B_{3u}3$	-48.926640	-	-48.898681
$^1B_{2u}1$	-50.754803	-	-50.736054
$^1B_{2u}2$	-49.604837	-	-49.640102
$^1B_{2u}3$	-49.062026	-	-49.049947
$^1B_{1g}1$	-50.314501	-	-50.381751
$^1B_{1g}2$	-49.866741	-	-49.875926
$^1B_{1g}3$	-48.929835	-	-48.990156
$^3B_{3u}1$	-50.522623	-	-50.508332
$^3B_{3u}2$	-49.965294	-	-49.989021
$^3B_{3u}3$	-49.526575	-	-49.543904
$^3B_{2u}1$	-52.625715	-	-52.598700
$^3B_{2u}2$	-50.828884	-	-50.788176
$^3B_{2u}3$	-49.839179	-	-49.761629
$^3B_{1g}1$	-51.664316	-	-51.654214
$^3B_{1g}2$	-50.106987	-	-50.083823
$^3B_{1g}3$	-49.740003	-	-49.739688

Table 3.10: Acene 5 standard

Poly-para-phenylenes

State	QCI	FCI	DMRG
$^1A_g1$	-25.276600	-25.300598	-25.301922
$^1A_g2$	-20.273411	-20.444224	-20.454111
$^1A_g3$	-19.389983	-19.524614	-19.531271
$^1B_{3u}1$	-20.439358	-20.451774	-20.463531
$^1B_{3u}2$	-19.517546	-19.675523	-19.686827
$^1B_{3u}3$	-19.101009	-19.164794	-19.172687
$^1B_{2u}1$	-21.566103	-21.691953	-21.697363
$^1B_{2u}2$	-19.548886	-19.729861	-19.737265
$^1B_{2u}3$	-19.504499	-19.573526	-19.577158
$^1B_{1g}1$	-21.558152	-21.684369	-21.689813
$^1B_{1g}2$	-19.587761	-19.731522	-19.738876
$^1B_{1g}3$	-19.547637	-19.652263	-19.655780
$^3B_{3u}1$	-22.697690	-22.744708	-22.774956
$^3B_{3u}2$	-21.546662	-21.651000	-21.670490
$^3B_{3u}3$	-20.262243	-20.417351	-20.437279
$^3B_{2u}1$	-21.544172	-21.640695	-21.646954
$^3B_{2u}2$	-20.191334	-20.347568	-20.360260
$^3B_{2u}3$	-20.091033	-20.140019	-20.143288
$^3B_{1g}1$	-21.543044	-21.639962	-21.646144
$^3B_{1g}2$	-20.193393	-20.349866	-20.362482
$^3B_{1g}3$	-20.076535	-20.125969	-20.129165

Table 3.11: PPP 2 screened

State	QCI	FCI	DMRG
$^1A_g1$	-28.760137	-28.767592	-28.767843
$^1A_g2$	-23.136526	-23.169327	-23.171134
$^1A_g3$	-23.025073	-23.091050	-23.093474
$^1B_{3u}1$	-23.942720	-23.949888	-23.952034
$^1B_{3u}2$	-22.551390	-22.574648	-22.578527
$^1B_{3u}3$	-22.280368	-22.336187	-22.339850
$^1B_{2u}1$	-24.657019	-24.700708	-24.701933
$^1B_{2u}2$	-22.225087	-22.299529	-22.301822
$^1B_{2u}3$	-22.126667	-22.155062	-22.156559
$^1B_{1g}1$	-24.628540	-24.671927	-24.673159
$^1B_{1g}2$	-22.481176	-22.506186	-22.507420
$^1B_{1g}3$	-22.227387	-22.300490	-22.302733
$^3B_{3u}1$	-25.636474	-25.651992	-25.660784
$^3B_{3u}2$	-24.618959	-24.653179	-24.658258
$^3B_{3u}3$	-23.156156	-23.207588	-23.213357
$^3B_{2u}1$	-24.590236	-24.621085	-24.622506
$^3B_{2u}2$	-23.472804	-23.487676	-23.488463
$^3B_{2u}3$	-23.013011	-23.067811	-23.071959
$^3B_{1g}1$	-24.589162	-24.620097	-24.621416
$^3B_{1g}2$	-23.434095	-23.449511	-23.450247
$^3B_{1g}3$	-23.019234	-23.074266	-23.078284

Table 3.12: PPP 2 standard

State	QCI	FCI	DMRG
$^1A_g1$	-38.203416	-	-38.270704
$^1A_g2$	-33.517632	-	-33.909513
$^1A_g3$	-32.631245	-	-32.962799
$^1B_{3u}1$	-33.917761	-	-34.022909
$^1B_{3u}2$	-32.886434	-	-33.287118
$^1B_{3u}3$	-32.108854	-	-32.412953
$^1B_{2u}1$	-34.392208	-	-34.566265
$^1B_{2u}2$	-34.202920	-	-34.773265
$^1B_{2u}3$	-32.587193	-	-32.832918
$^1B_{1g}1$	-34.155958	-	-34.566200
$^1B_{1g}2$	-32.542788	-	-32.833733
$^1B_{1g}3$	-32.485042	-	-32.824832
$^3B_{3u}1$	-35.687638	-	-35.881183
$^3B_{3u}2$	-34.683248	-	-35.058415
$^3B_{3u}3$	-34.306740	-	-34.665373
$^3B_{2u}1$	-34.395798	-	-34.494016
$^3B_{2u}2$	-34.224587	-	-34.701800
$^3B_{2u}3$	-33.129854	-	-33.353631
$^3B_{1g}1$	-34.182725	-	-34.494144
$^3B_{1g}2$	-33.173001	-	-33.217804
$^3B_{1g}3$	-32.896993	-	-33.166982

Table 3.13: PPP 3 screened

State	QCI	FCI	DMRG
$^1A_g1$	-43.450717	-	-43.471272
$^1A_g2$	-38.121553	-	-38.276099
$^1A_g3$	-38.097122	-	-38.244591
$^1B_{3u}1$	-39.021531	-	-39.066661
$^1B_{3u}2$	-37.734200	-	-37.831553
$^1B_{3u}3$	-37.527501	-	-37.683912
$^1B_{2u}1$	-39.349500	-	-39.509281
$^1B_{2u}2$	-39.194809	-	-39.349549
$^1B_{2u}3$	-37.248064	-	-37.384462
$^1B_{1g}1$	-39.179264	-	-39.350968
$^1B_{1g}2$	-36.996591	-	-37.148503
$^1B_{1g}3$	-36.984715	-	-37.089500
$^3B_{3u}1$	-40.476097	-	-40.548155
$^3B_{3u}2$	-39.573657	-	-39.716053
$^3B_{3u}3$	-39.246475	-	-39.389047
$^3B_{2u}1$	-39.304023	-	-39.269880
$^3B_{2u}2$	-39.170955	-	-39.428875
$^3B_{2u}3$	-38.273008	-	-38.361988
$^3B_{1g}1$	-39.153565	-	-39.269825
$^3B_{1g}2$	-38.076551	-	-38.171140
$^3B_{1g}3$	-37.813777	-	-38.031123

Table 3.14: PPP 3 standard

Trigonal zigzag graphene nanodisks

System	Parameters	A_1	B_2
TZGND-1 doublet	Screened	-25.784324	-27.793568
		-25.366065	-25.786939
		-24.404038	-24.409357
	Standard	-29.160049	-31.379637
		-28.728226	-29.160574
		-27.792477	-27.635932
TZGND-2 singlet	Screened	-47.682268	-47.682346
		-45.908450	-45.907757
		-45.596365	-45.596343
	Standard	-53.830723	-53.830848
		-51.876156	-51.876491
		-51.559202	-51.559564
TZGND-2 triplet	Screened	-45.922645	-48.201089
		-45.764165	-46.057782
		-45.441111	-45.841121
	Standard	-52.021886	-54.359609
		-51.804331	-52.081932
		-51.520589	-51.847026

Table 3.15: TZGND gound and excited state DMRG energies

Bibliography

[1] Garnet Kin-Lic Chan and Sandeep Sharma. "The density matrix renormalization group in quantum chemistry". In: *Annual review of physical chemistry* 62 (2011), pp. 465–481.

[2] Debashree Ghosh et al. "Orbital optimization in the density matrix renormalization group, with applications to polyenes and β-carotene". In: *The Journal of chemical physics* 128.14 (2008), p. 144117.

[3] Roger A Horn and Charles R Johnson. *Matrix analysis*. Cambridge university press, 2012.

[4] Michael A Nielsen and Isaac L Chuang. *Quantum computation and quantum information*. Cambridge university press, 2010.

[5] Roberto Olivares-Amaya et al. "The ab-initio density matrix renormalization group in practice". In: *The Journal of chemical physics* 142.3 (2015), p. 034102.

[6] Román Orús. "A practical introduction to tensor networks: Matrix product states and projected entangled pair states". In: *Annals of Physics* 349 (2014), pp. 117–158.

[7] Stellan Östlund and Stefan Rommer. "Thermodynamic Limit of Density Matrix Renormalization". In: *Phys. Rev. Lett.* 75 (19 1995), pp. 3537–3540. DOI: 10.1103/PhysRevLett.75.3537. URL: http://link.aps.org/doi/10.1103/PhysRevLett.75.3537.

[8] Ulrich Schollwöck. "The density-matrix renormalization group". In: *Reviews of modern physics* 77.1 (2005), p. 259.

[9] Ulrich Schollwöck. "The density-matrix renormalization group in the age of matrix product states". In: *Annals of Physics* 326.1 (2011), pp. 96–192.

[10] Sandeep Sharma and Garnet Kin-Lic Chan. "Spin-adapted density matrix renormalization group algorithms for quantum chemistry". In: *The Journal of chemical physics* 136.12 (2012), p. 124121.

[11] Priya Sony and Alok Shukla. "A general purpose Fortran 90 electronic structure program for conjugated systems using Pariser–Parr–Pople model". In: *Computer Physics Communications* 181.4 (2010), pp. 821–830.

[12] Attila Szabo and Neil S Ostlund. *Modern quantum chemistry: introduction to advanced electronic structure theory*. Courier Corporation, 2012.

[13] Steven R White. "Density-matrix algorithms for quantum renormalization groups". In: *Physical Review B* 48.14 (1993), p. 10345.

[14] Steven R White. "Density matrix formulation for quantum renormalization groups". In: *Physical Review Letters* 69.19 (1992), p. 2863.

[15] Steven R White and Richard L Martin. "Ab initio quantum chemistry using the density matrix renormalization group". In: *The Journal of chemical physics* 110.9 (1999), pp. 4127–4130.

[16] Sebastian Wouters and Dimitri Van Neck. "The density matrix renormalization group for ab initio quantum chemistry". In: *European Physical Journal D* 68.9 (2014), p. 272. DOI: 10.1140/epjd/e2014-50500-1.

[17] Sebastian Wouters et al. "CheMPS2: a free open-source spin-adapted implementation of the density matrix renormalization group for ab initio quantum chemistry". In: *Computer Physics Communications* 185.6 (2014), pp. 1501–1514. DOI: 10.1016/j.cpc.2014.01.019.

[18] Sebastian Wouters et al. "Communication: DMRG-SCF study of the singlet, triplet, and quintet states of oxo-Mn(Salen)". In: *Journal of Chemical Physics* 140.24 (2014), p. 241103. DOI: 10.1063/1.4885815.